

---

# BAYESIAN COMPOSITIONAL REGRESSION WITH FLEXIBLE MICROBIOME FEATURE AGGREGATION AND SELECTION

---

A PREPRINT

**Satabdi Saha**

Department of Biostatistics  
The University of Texas MD Anderson Cancer Center,  
Houston, TX  
ssaha1@mdanderson.org

**Liangliang Zhang**

Department of Population and Quantitative Health Sciences  
Case Western Reserve University  
Cleveland, OH  
lxz716@case.edu

**Kim-Anh Do**

Department of Biostatistics  
The University of Texas MD Anderson Cancer Center,  
Houston, TX  
kimdo@mdanderson.org

**Christine B. Peterson**

Department of Biostatistics  
The University of Texas MD Anderson Cancer Center,  
Houston, TX  
cbpeterson@mdanderson.org

November 18, 2024

## ABSTRACT

Ongoing advances in microbiome profiling have allowed unprecedented insights into the molecular activities of microbial communities. This has fueled a strong scientific interest in understanding the critical role the microbiome plays in governing human health, by identifying microbial features associated with clinical outcomes of interest. Several aspects of microbiome data limit the applicability of existing variable selection approaches. In particular, microbiome data are high-dimensional, extremely sparse, and compositional. Importantly, many of the observed features, although categorized as different taxa, may play related functional roles. To address these challenges, we propose a novel compositional regression approach that leverages the data-adaptive clustering and variable selection properties of the spiked Dirichlet process to identify taxa that exhibit similar functional roles. Our proposed method, Bayesian Regression with Agglomerated Compositional Effects (BRACE), enables the identification of a sparse set of features with shared impacts on the outcome, facilitating dimension reduction and model interpretation. We demonstrate that BRACE outperforms existing approaches for microbiome variable selection through simulation studies and an application elucidating the impact of oral microbiome composition on insulin resistance.

## 1 Introduction

The microbiome, an incredibly diverse community of organisms, plays a pivotal role in human health and disease (Pflughoeft & Versalovic 2012). Microbiome composition is highly heterogeneous, with notable diversity across individuals shaped by factors such as environment and dietary habits. Recent scientific studies have associated taxonomic or functional changes in the microbiome with a spectrum of health conditions. In particular, oral microbial abundances have been shown to correlate with systemic inflammation and insulin resistance (Demmer et al. 2017).

The methodological developments proposed in this work are motivated by the Oral Infections, Glucose Intolerance, and Insulin Resistance Study (ORIGINS) (Demmer et al. 2015), which seeks to characterize the association between the bacterial population of subgingival plaque and prediabetes. Oral microorganisms play a key role in shaping the risk of periodontal diseases, including periodontitis (Pihlstrom et al. 2005). It is postulated that chronic inflammation driven by the periodontal microbiota may contribute to impaired glucose regulation and heightened risk of insulin resistance, potentially laying the groundwork for type 2 diabetes (Gurav 2012). Through our case study on the ORIGINS data, we aim to identify taxa associated with insulin resistance, shedding light on the influence of the periodontal microbiome on prediabetes.

In recent years, technological advancements have enabled direct quantification of microbiome composition. Most microbiome studies rely on sequencing of the 16S ribosomal RNA (rRNA) gene, which functions as a barcode that can be used to identify the bacterial species present in a sample. The analysis of microbiome profiling data poses numerous challenges (Peterson et al. 2024). First, due to limitations in sample collection and sequencing, the observed abundances can be interpreted only on a relative, rather than an absolute, scale. This characteristic renders the data inherently compositional and necessitates specialized analytical approaches (Gloor et al. 2017). Moreover, the high dimensionality of microbiome data necessitates sparse modeling techniques to identify relevant features for the prediction of clinical outcomes (Lin et al. 2014). Finally, microbiome data sets contain numerous rare features, for instance, those observed in less than 5% or 10% of subjects. Typically, these rare features are filtered out prior to downstream analysis (Callahan et al. 2016). An alternative approach to filtering is to group features at higher taxonomic levels, using taxonomic trees that follow the traditional hierarchical classification *Kingdom, Phylum, Class, Order, Family, Genus, Species*. Phylogenetic trees, which can be obtained via bioinformatic pipelines, can also be used instead, to group features on the basis of their potential evolutionary relationships, and may be integrated into analysis as an external source of information on feature similarity.

Understanding the role of the microbiome in regulating human health outcomes can be approached as a regression problem with compositional predictors. In early work on compositional data analysis, Aitchison & Bacon-Shone (1984) proposed the linear log-contrast model for regression modeling with compositional covariates. Building on that idea, Lin et al. (2014) proposed applying an  $l_1$  penalty to the coefficient vector of the linear log contrast model for sparse estimation of coefficients and improved prediction accuracy in the context of high-dimensional data. Shi et al. (2016) extended this work by selecting subcompositions of taxa at fixed taxonomic levels. Zhang et al. (2021) proposed a Bayesian model where the compositionality constraint was incorporated in the prior for the coefficient vector through a conditioning matrix with a controllable shrinkage parameter. To encourage joint selection of phylogenetically related features, the authors incorporated information from a known phylogenetic tree through an Ising prior. Zhang et al. (2024) proposed a Bayesian compositional generalized linear model that incorporates the phylogenetic relatedness among taxa through a structured regularized horseshoe prior. To deal with rare features, Bien et al. (2021) proposed grouping finer-resolution taxa into higher levels of taxonomic resolution by aggregating features over branches of a known tree and using the aggregated features in the outcome prediction.

However, these existing modeling approaches have critical limitations. The penalty-based methods proposed by Lin et al. (2014) and Shi et al. (2016) provide point estimates of regression coefficients that do not fully capture the uncertainty. In addition, these methods are optimized for prediction, rather than feature selection, and tend to have relatively high false positive rates (Zhang et al. 2021). The Bayesian approach proposed by Zhang et al. (2021) requires external information about a phylogenetic tree for estimation; this information reflects global genomic similarity between species, which may be an imperfect or noisy reflection of their functional similarity in driving an outcome of interest. Although Bien et al. (2021) account for the presence of rare features, they similarly rely on a fixed externally defined tree to achieve feature aggregation.

In this article, we introduce Bayesian Regression with Agglomerated Compositional Effects (BRACE), a framework tailored for analyzing microbiome data that adeptly navigates inherent challenges such as its compositional structure, high dimensionality, and rare features. To effectively address the fixed-sum constraint, we develop a novel spiked Dirichlet process prior with a constrained multivariate normal base distribution for the regression coefficients. This approach enables the direct sampling of compositionally constrained regression coefficients within the Gibbs sampling framework, building on recent advances in sampling truncated normal densities. Additionally, our proposed method enables simultaneous variable selection and natural clustering of compositional microbiome profiles, effectively tackling

the challenge posed by rare features. Through clustering the coefficients of sparsely observed features, we achieve substantial dimension reduction, resulting in denser features representing groups of organisms with shared effects, ultimately enhancing the prediction of clinical outcomes. Our innovative approach clusters regression coefficients in a data-adaptive manner, strategically collapsing rare features to generate denser groupings. To the best of our knowledge, BRACE stands as the first Bayesian method for high-dimensional compositional regression with flexible microbiome feature aggregation and selection.

The remainder of the article is organized as follows: In Section 2, we provide a description of the proposed model and estimation procedure. In Section 3, we benchmark the performance of BRACE against alternative approaches through simulation studies. In Section 4, we demonstrate the applicability of BRACE through a study that aims to capture the relationship between subgingival microbial community composition and insulin resistance. Finally, Section 5 includes a discussion and concluding remarks.

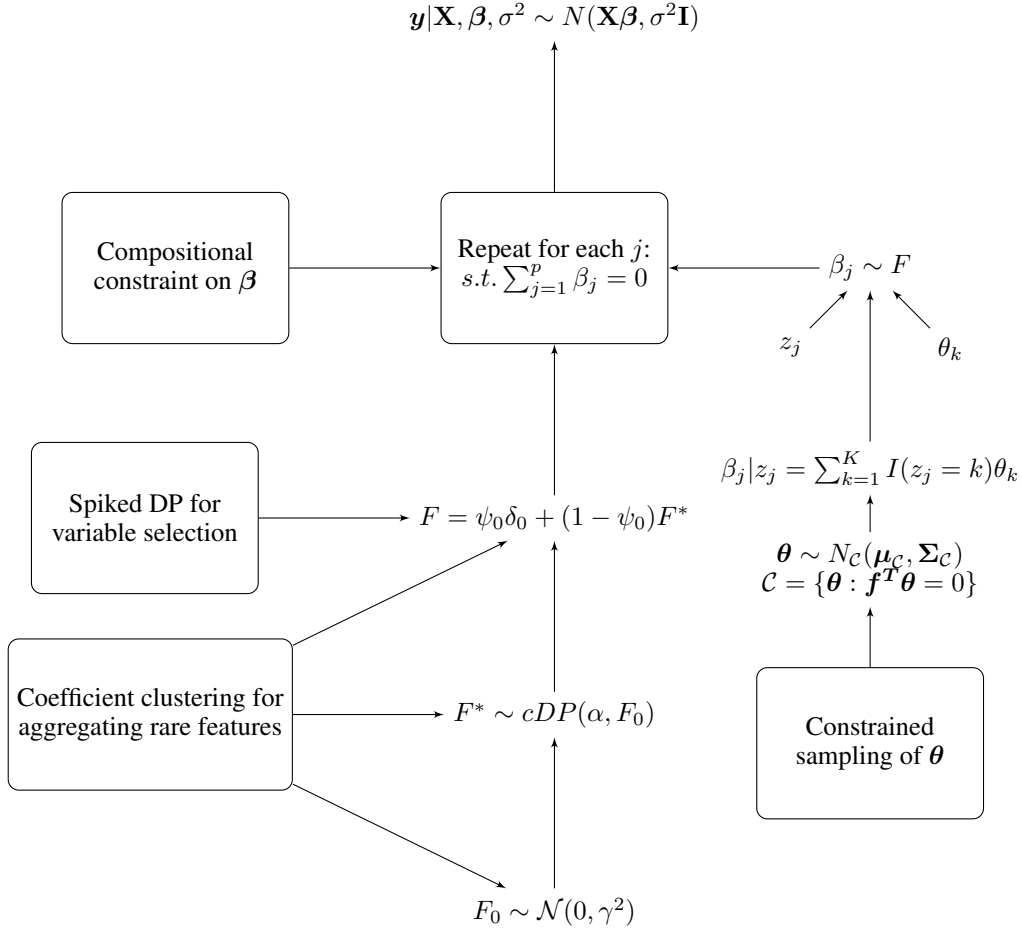


**Figure 1:** Overview figure for Bayesian compositional regression for high dimensional clustered effects

## 2 Methods

### 2.1 Background

BRACE builds on the compositional regression framework for the prediction of continuous outcomes from microbiome profiles. Let  $\mathbf{y} = \{y_1, \dots, y_n\}$  denote the vector of continuous responses across  $n$  subjects, and  $\mathbf{U}$  denote the  $n \times p$  observed microbial abundance matrix for  $p$  features. Notably, the sequencing methods used for generating the microbial abundances result in compositional data. Consequently, the observed counts are only interpretable on a relative scale, emphasizing their proportional rather than absolute nature. Prior to downstream analysis, the observed abundance tables are generally converted to relative abundance matrices using a data transformation. To avoid numerical issues, the exact zeroes in the count matrix are generally replaced with a pseudocount of 0.5. To obtain the relative abundances, we rely on total sum scaling, where each element of the count matrix  $u_{ij}$  is divided by its sample sum  $\sum_{j=1}^p u_{ij}$ . The resulting

relative abundance matrix  $\tilde{\mathbf{U}}$  satisfies the compositional constraint  $\sum_{j=1}^p \tilde{u}_{ij} = 1$ . Each row of  $\tilde{\mathbf{U}}$  is constrained to the simplex  $\mathcal{S}^p$ , rather than the unrestricted real space  $\mathbb{R}^p$ .  $\tilde{\mathbf{U}}$  is then log transformed to obtain the log relative abundance matrix  $\mathbf{X}$ , where  $\mathbf{X} = \log(\tilde{\mathbf{U}})$ . Importantly, the  $p$  features in the matrix  $\mathbf{X}$  are still dependent due to the original compositionality constraint.

We now consider the formulation of the regression model relating the compositional microbiome data  $\mathbf{X}$  to the vector of clinical outcomes  $\mathbf{y}$ . To deal with compositional covariates, Aitchison & Bacon-Shone (1984) proposed the linear log-contrast model:

$$\mathbf{y} = \mathbf{C}_{\setminus p} \boldsymbol{\beta}_{\setminus p} + \boldsymbol{\varepsilon}, \quad (1)$$

where  $\mathbf{C}_{\setminus p} = \log(u_{ij}/u_{ip})$  is an  $n \times (p-1)$  matrix of the additive log-ratio transformed predictor variables, with the transformation done using the  $p^{\text{th}}$  predictor as the reference component,  $\boldsymbol{\beta}_{\setminus p} = \{\beta_1, \dots, \beta_{p-1}\}$  is the vector of  $p-1$  regression coefficients, and the entries in the noise vector are distributed independently as  $\varepsilon_i \sim \mathcal{N}(0, \sigma^2)$ , for  $i = 1, \dots, n$ . To eliminate the need to select a reference component, we consider an equivalent representation, (Lin et al. 2014):

$$\mathbf{y} = \mathbf{X}\boldsymbol{\beta} + \boldsymbol{\varepsilon} \quad \text{subject to the constraint} \quad \mathbf{1}^T \boldsymbol{\beta} = 0. \quad (2)$$

The intercept term is omitted by centering the response and predictor variables. Our goal is to make inference on the regression coefficients  $\boldsymbol{\beta}$  based on the observed data  $(\mathbf{y}, \mathbf{X})$  where it is assumed that any prior on  $\boldsymbol{\beta}$  satisfies  $Pr(\mathcal{S}) = 1$ , where  $\mathcal{S} = \{\boldsymbol{\beta} : \mathbf{1}^T \boldsymbol{\beta} = 0\}$ . It is important to note that when the model coefficients should satisfy the constraint  $\mathbf{1}^T \boldsymbol{\beta} = 0$ , using unrestricted priors on  $\boldsymbol{\beta}$  (such as a standard multivariate normal or continuous shrinkage priors) can lead to a loss of finite sample efficiency for the parameter estimates by disregarding this structural constraint. In addition, the posterior distribution of  $\boldsymbol{\beta}$  might assign probability mass to regions of the parameter space that are not feasible under the true model, ultimately leading to invalid parameter estimates.

Another important consideration in modelling microbiome data is the presence of highly sparse features. To improve signal, a common approach is to group finer-resolution taxa into higher levels of taxonomic resolution by summing over all the features that belong to the corresponding classification in a known taxonomic tree. More generally, suppose we obtain a new aggregated feature for the  $i$ th subject  $x_{i,a} = x_{i,1} + x_{i,2} + \dots + x_{i,m}$ , where  $m$  denotes the number of leaf nodes descending from the ancestor node  $a$ . As noted in Yan & Bien (2021), in the linear model setting,  $x_{i,a}\boldsymbol{\beta} = (x_{i,1} + x_{i,2} + \dots + x_{i,m})\boldsymbol{\beta} = x_{i,1}\boldsymbol{\beta} + x_{i,2}\boldsymbol{\beta} + \dots + x_{i,m}\boldsymbol{\beta}$ . Effectively, this means that learning a model where some features have exactly equal coefficients  $\boldsymbol{\beta}$  corresponds to aggregation of the original rare features into a smaller set of more common features. A key limitation of Bien et al. (2021) is that they assume that this aggregation must occur within branches of a known tree structure; this assumption is overly rigid, as any external tree structure will not precisely reflect the target of interest, which is similarity of effects on the regression outcome.

We instead propose to employ a prior distribution on  $\boldsymbol{\beta}$  that effectively constrains the parameter space while allowing for rare feature aggregation. To ensure data-adaptive clustering of the coefficients and to enable simultaneous feature selection, we propose a compositionally-constrained spiked Dirichlet process prior on the model coefficients. This strategy allows coefficients that cluster together to correspond to features that can be aggregated, providing flexibility in identifying sets of features with similar impacts on the outcome. Additionally, the spike allows clustering of the nonzero values, thus imposing sparsity. We now provide the mathematical formulation of our proposed model.

## 2.2 Model Specification

We propose the the following model which entails a spiked Dirichlet process prior subject to linear equality constraints. We refer to this formulation as a spiked constrained Dirichlet process (cDP):

$$\begin{aligned} \mathbf{y} | \mathbf{X}, \boldsymbol{\beta}, \sigma^2 &\sim N(\mathbf{X}\boldsymbol{\beta}, \sigma^2 \mathbf{I}) \\ \boldsymbol{\beta}_j | F &\sim F \quad \text{s.t.} \quad \sum_{j=1}^p \boldsymbol{\beta}_j = 0, \\ F &\sim \text{cDP}(\psi_0, \alpha, F_0). \end{aligned} \quad (3)$$

Here,  $F$  resembles a spiked Dirichlet process (DP) prior (Dunson et al. 2008) that uses a mixture of a point mass at zero with a distribution given by a DP prior. In this formulation, the parameter  $\psi_0$  is the prior probability of a coefficient being exactly zero, arising from a Dirac delta ‘‘spike’’  $\delta_0$ . A standard DP prior is characterized by a concentration parameter  $\alpha$ , which is a scalar controlling the degree of discretization, and a base distribution  $F_0$ , i.e.,  $E(F) = F_0$ .

Mathematically, we can write our spiked cDP as:

$$\begin{aligned} F &= \psi_0 \delta_0 + (1 - \psi_0) F^*, \\ F^* &\sim cDP(\alpha, F_0), \\ [\psi_0, (1 - \psi_0)] &\sim \text{Dirichlet}\left(\frac{\alpha_0}{2}, \frac{\alpha_0}{2}\right). \end{aligned} \quad (4)$$

A key property of the Dirichlet process is that  $F$  is almost surely discrete, even if the base measure is continuous. Therefore, given an initial value for the set of regression coefficients  $\beta = (\beta_1, \dots, \beta_p)$ , we can define  $\theta = (\theta_1, \dots, \theta_K)$  as the set of  $K$  distinct elements of  $\beta$ . Since the discreteness of the Dirichlet process will induce some repeated elements in  $\beta$ ,  $K$  will be generally smaller than  $p$ . We define the latent vector  $z = (z_1, \dots, z_p)$  such that  $z_j = k$  if  $\beta_j = \theta_k$ . Using  $z$ , as the cluster labels of the regression coefficient vector  $\beta$ , and  $\theta$ , as the corresponding cluster parameters, the prior on  $\beta$  can be reparametrized as:

$$f(\theta, z | \gamma^2, \alpha) = p(z | \alpha) f(\theta | \gamma^2, z). \quad (5)$$

This prior structure follows directly from the Pólya urn representation of the Dirichlet process (Blackwell & MacQueen 1973). Essentially, for the predictor variables,  $j \in \{1, \dots, p\}$ ,  $\beta_j | z_j = \sum_{k=1}^K I(z_j = k) \theta_k$ ; where  $k = 1, 2, \dots, K$  represent the unique cluster labels in  $z$ . To accommodate the constraint  $\mathbf{1}^T \beta = 0$  under the reparametrized model, we first define the probability density function of a truncated normal distribution where  $\mathbf{b} \sim \mathcal{TN}_p(\boldsymbol{\mu}, \boldsymbol{\Sigma}, \mathbf{H}, \mathbf{q})$ ,

$$f(\mathbf{b}) = \frac{\exp\left\{-\frac{1}{2}(\mathbf{b} - \boldsymbol{\mu})^T \boldsymbol{\Sigma}^{-1}(\mathbf{b} - \boldsymbol{\mu})\right\}}{\int_{\mathbf{H}\mathbf{b}=\mathbf{q}} \exp\left\{-\frac{1}{2}(\mathbf{b} - \boldsymbol{\mu})^T \boldsymbol{\Sigma}^{-1}(\mathbf{b} - \boldsymbol{\mu})\right\} d\mathbf{b}} I(\mathbf{H}\mathbf{b} = \mathbf{q}), \quad (6)$$

where  $\mathbf{H}$  is an  $m \times p$  projection matrix,  $\mathbf{q}$  is a constraint vector of length  $m$ , and  $I(\cdot)$  is an indicator function such that  $I(x) = 1$  if condition  $x$  is satisfied, otherwise  $I(x) = 0$ . To satisfy the compositional constraint, we would like the clustered values in  $\beta$  to sum to 0, which in turn translates to a truncated multivariate normal prior on  $\theta$  as

$$\theta | z, \gamma^2 \sim \mathcal{TN}(\boldsymbol{\mu}, \boldsymbol{\Sigma}, \mathbf{f}^T, 0). \quad (7)$$

Since in our case,  $m = 1$ ,  $\mathbf{H}$  becomes a vector and  $\mathbf{q}$  is a scalar. For our formulation,  $q = 0$  and  $\mathbf{H}$  is the  $K$ -vector  $\mathbf{f}^T$ , where  $f_k = \sum_{j=1}^p I(z_j = k)$  and  $k = 1, 2, \dots, K$  are the unique cluster labels in  $z$ , i.e., the  $k^{\text{th}}$  element of  $\mathbf{f}$  corresponds to the number of elements in the  $k^{\text{th}}$  cluster.

### Illustration of prior

Here, we provide a simple illustration of the prior on  $\theta$ . Let  $\theta = \{\theta_1, \theta_2, \theta_3\}$  and  $z = \{1, 1, 1, 2, 2, 3\}$ . Then  $\beta_j | z_j = \sum_{k=1}^K I(z_j = k) \theta_k$ , so that  $\beta = \{\theta_1, \theta_1, \theta_1, \theta_2, \theta_2, \theta_3\}$ . In order to satisfy the compositionality constraint, we require that  $\mathbf{1}^T \beta = 0$  which implies that  $\mathbf{f}^T \theta = 0$  where  $\mathbf{f}^T = (3, 2, 1)$ . This serves as our new constraint under the reparametrized model.

Next, we provide a complete formulation of BRACE's hierarchical structure:

$$\begin{aligned} \mathbf{y} | \mathbf{X}, \boldsymbol{\beta}, \sigma^2 &\sim N(\mathbf{X}\boldsymbol{\beta}, \sigma^2 \mathbf{I}) \\ \boldsymbol{\beta} &\sim \psi_0 \delta_0 + (1 - \psi_0) F^* \\ F^* &\sim cDP(\alpha, F_0) \\ F_0 &\sim \mathcal{TN}(\mathbf{0}, \gamma^2 \mathbf{I}, \mathbf{f}^T, 0) \\ [\psi_0, (1 - \psi_0)] &\sim \text{Dirichlet}\left(\frac{\alpha_0}{2}, \frac{\alpha_0}{2}\right). \end{aligned} \quad (8)$$

In this formulation, the dependence induced by the sum constraint in equation (3) has been removed, and the compositional constraint is now expressed through the truncation of the base distribution. To complete the model formulation, we place standard Inverse Gamma hyperpriors on the variance parameters,  $\sigma^2 \sim IG(a_\sigma, b_\sigma)$  and  $\gamma^2 \sim IG(a_\gamma, b_\gamma)$  and a non-informative Gamma prior on the concentration parameter,  $\alpha \sim \text{Gamma}(a_\alpha, b_\alpha)$ .

### 2.3 Posterior inference

To perform posterior inference for our proposed model, we employ a Gibbs sampler to iteratively draw samples from the posterior full conditional distributions of the parameters. Next, we define the Gibbs sampling steps for our model.

### 2.3.1 Sampling of the cluster labels $\mathbf{z}$

From the reparametrized model in equation (5), it is clear that given  $\mathbf{z}$ , we need to estimate only  $K$  nonzero coefficients  $\boldsymbol{\theta}$ . We define the  $p \times K$  cluster membership matrix  $\mathbf{Z}$  such that  $\mathbf{Z}_{jk} = 1$  if  $z_j = k$ , and 0 otherwise (Mehrotra & Maity 2022). To update the cluster label  $z_j$  for predictor  $j$ , we need to calculate the posterior probability of predictor  $j$  belonging to each cluster. We update  $\mathbf{z}$  to  $\mathbf{z}^*$  where

$$P(z_j = k | \mathbf{z}_{-j}, \gamma^2, \sigma^2, \alpha, \boldsymbol{\theta}, \mathbf{X}, \mathbf{y}) \propto P(z_j = k | \mathbf{z}_{-j}, \alpha) f(\mathbf{y} | \gamma^2, \sigma^2, \mathbf{X}, \mathbf{z}^*) \quad (9)$$

where  $\mathbf{z}^*$  is the vector of class labels with  $z_j = k$ . In order add a spike for allowing variable selection, the stick breaking view of the DP process can be reformulated to include a cluster containing only zeroes (Dunson et al. 2008). This induces a natural clustering of the coefficients, while allowing for sparsity in the presence of compositionality. A DP process  $F^*$  can be expressed as the infinite sum:  $F^* = \sum_{k=1}^{\infty} \psi_k \delta_{\theta_k}$ , where  $\delta_{\theta_k}$  is the indicator function that evaluates to zero everywhere except for  $\delta_{\theta_k}(\theta_k) = 1$ ,  $\psi_k = V_k \sum_{l=1}^{k-1} (1 - V_l)$ ,  $V_k \sim \text{Beta}(1, \alpha)$ , and  $\theta_k \sim F_0$ , for  $k \geq 1$ . Therefore, for the spiked DP process, we can write:

$$\begin{aligned} F &= \psi_0 \delta_0 + (1 - \psi_0) F^* \\ &= \psi_0 \delta_0 + (1 - \psi_0) \sum_{k=1}^{\infty} \psi_k \delta_{\theta_k} \\ &= \sum_{k=0}^{\infty} \tilde{\psi}_k \delta_{\theta_k}, \end{aligned} \quad (10)$$

where  $\tilde{\psi}_0 = \psi_0$ ,  $\tilde{\psi}_k = (1 - \psi_0) \psi_k$ , and  $\theta_0 = 0$ . The spiked DP prior is therefore a special case of the DP prior, with the specific limitation that the first cluster equals zero. For the spiked DP model, the constraint for the zeroth cluster can be accounted for in equation (9) by dropping the columns in the zero cluster from  $\mathbf{X}$ , since their effects are restricted to be zero. If we define  $p = p_0 + p_z$ , where  $p_0$  is the number of variables in the zeroth cluster and  $p_z$  is the number of elements in the nonzero clusters, then  $\psi_0 = P(z_j = 0 | \mathbf{z}_{-j}, \alpha_0)$  can be sampled and the prior for  $\mathbf{z}$  can be modified as described in Neal (2000):

$$\begin{aligned} \psi_0 &= P(z_j = 0 | \mathbf{z}_{-j}, \alpha_0) = \frac{m_{-j,0} + \alpha_0/2}{p - 1 + \alpha_0} \\ \text{For } K \geq 1, P(z_j = k | \mathbf{z}_{-j}, \alpha) &= (1 - \psi_0) \frac{m_{-j,k}}{p_z - 1 + \alpha} \\ P(z_j \neq z_l, \forall j \neq l | \mathbf{z}_{-j}, \alpha) &= (1 - \psi_0) \frac{\alpha}{p_z - 1 + \alpha} \end{aligned} \quad (11)$$

Next, we need to compute the conditional distribution of  $\mathbf{y}$  to characterize the Gibbs step for sampling the cluster labels  $\mathbf{z}$  using equation (9). This step employs a collapsed Gibbs sampling approach, where we analytically integrate out the parameter  $\boldsymbol{\theta}$ . By marginalizing over  $\boldsymbol{\theta}$ , we reduce the dimensionality of the sampling space, which can significantly improve the mixing properties of the Markov chain.

$$\begin{aligned} f(\mathbf{y} | \sigma^2, \gamma^2, \mathbf{z}, \mathbf{X}) &= \int (2\pi\sigma^2)^{-n/2} \exp \left\{ -\frac{1}{2\sigma^2} (\mathbf{y} - \mathbf{X}_z \boldsymbol{\theta})^T (\mathbf{y} - \mathbf{X}_z \boldsymbol{\theta}) \right\} \times \\ &\quad \frac{\exp \left\{ -\frac{1}{2\gamma^2} \boldsymbol{\theta}^T \boldsymbol{\theta} \right\}}{\int_{\mathbf{f}^T \boldsymbol{\theta} = 0} \exp \left\{ -\frac{1}{2\gamma^2} \boldsymbol{\theta}^T \boldsymbol{\theta} \right\} d\boldsymbol{\theta}} I(\mathbf{f}^T \boldsymbol{\theta} = 0) d\boldsymbol{\theta} \end{aligned} \quad (12)$$

Note that  $\mathbf{f}^T \boldsymbol{\theta} = 0 \implies \sum_{k=1}^K f_k \theta_k = 0 \implies \theta_K = -\frac{1}{f_K} \sum_{k=1}^{K-1} f_k \theta_k$ . First, we compute the normalizing constant for the truncated normal distribution:

$$\begin{aligned} &\int_{\mathbf{f}^T \boldsymbol{\theta} = 0} \exp \left\{ -\frac{1}{2\gamma^2} \boldsymbol{\theta}^T \boldsymbol{\theta} \right\} d\boldsymbol{\theta} \\ &= \int_{\mathbb{R}^{K-1}} \exp \left( -\frac{1}{2\gamma^2} \boldsymbol{\theta}^{*T} \mathbf{B} \boldsymbol{\theta}^* \right) d\boldsymbol{\theta}^*, \\ &= \sqrt{\frac{(2\pi\gamma^2)^{K-1}}{\det(\mathbf{B})}}. \end{aligned} \quad (13)$$

where  $\boldsymbol{\theta}^* = \{\theta_1, \dots, \theta_{K-1}\}$  and  $\mathbf{f}^* = \{f_1, \dots, f_{K-1}\}$ ,  $\mathbf{B} = \mathbf{I} + \frac{\mathbf{f}^* \mathbf{f}^{*T}}{f_K^2}$  and  $\mathbf{I}$  is the  $(K-1) \times (K-1)$  identity matrix. We now show that  $\det(\mathbf{B})$  has a simple analytic form. Let  $\mathbf{v} = \frac{\mathbf{f}^*}{f_K^2}$  and  $\mathbf{u} = \mathbf{f}^*$ . By the Weinstein–Aronszajn identity,  $\det(\mathbf{I} + \mathbf{u}\mathbf{v}^T) = \det(1 + \mathbf{v}^T \mathbf{u}) = 1 + \mathbf{v}^T \mathbf{u}$ . We can therefore write  $\det(\mathbf{B}) = \det\left(\mathbf{I} + \frac{\mathbf{f}^* \mathbf{f}^{*T}}{f_K^2}\right) = 1 + \frac{\mathbf{f}^{*T} \mathbf{f}^*}{f_K^2} = \frac{\sum_{k=1}^K f_k^2}{f_K^2}$ .

Next we compute the integral over the remaining terms in equation (12),

$$\begin{aligned} & \int_{\boldsymbol{\theta}} \exp\left\{-\frac{1}{2\sigma^2}(\mathbf{y} - \mathbf{X}_z \boldsymbol{\theta})^T (\mathbf{y} - \mathbf{X}_z \boldsymbol{\theta})\right\} \times \exp\left\{-\frac{1}{2\gamma^2} \boldsymbol{\theta}^T \boldsymbol{\theta}\right\} I(\mathbf{f}^T \boldsymbol{\theta} = 0) d\boldsymbol{\theta} \\ &= \exp\left\{-\frac{\mathbf{y}^T \mathbf{y}}{2\sigma^2}\right\} \times \int_{\boldsymbol{\theta}} \exp\left\{-\frac{1}{2\sigma^2}(\boldsymbol{\theta}^T \mathbf{A} \boldsymbol{\theta} - 2\mathbf{b}^T \boldsymbol{\theta})\right\} I(\mathbf{f}^T \boldsymbol{\theta} = 0) d\boldsymbol{\theta}, \end{aligned} \quad (14)$$

where  $\mathbf{z}^*$  is the vector of class labels with  $z_j = k$  and  $\mathbf{X}_z = \mathbf{X}\mathbf{Z}^*$ ,  $\mathbf{A} = \mathbf{X}_z^T \mathbf{X}_z + \frac{\sigma^2}{\gamma^2} \mathbf{I}$ , and  $\mathbf{b} = \mathbf{X}_z^T \mathbf{y}$ . To evaluate the integral

$$\int_{\mathbf{f}^T \boldsymbol{\theta} = 0} \exp\left\{-\frac{1}{2\sigma^2}(\boldsymbol{\theta}^T \mathbf{A} \boldsymbol{\theta} - 2\mathbf{b}^T \boldsymbol{\theta})\right\} d\boldsymbol{\theta},$$

we rewrite the terms involving  $\boldsymbol{\theta}$ , which is subject to a constraint, in terms of the unconstrained vector  $\boldsymbol{\theta}^*$ . To rewrite the first term, we note that

$$\boldsymbol{\theta}^T \mathbf{A} \boldsymbol{\theta} = \begin{pmatrix} \boldsymbol{\theta}^* \\ -\frac{1}{f_K} \mathbf{f}^{*T} \boldsymbol{\theta}^* \end{pmatrix}^T \begin{pmatrix} \mathbf{A}_{11} & \mathbf{A}_{12} \\ \mathbf{A}_{12}^T & a_{KK} \end{pmatrix} \begin{pmatrix} \boldsymbol{\theta}^* \\ -\frac{1}{f_K} \mathbf{f}^{*T} \boldsymbol{\theta}^* \end{pmatrix},$$

where  $\mathbf{A}_{11}$  is a  $(K-1) \times (K-1)$  matrix,  $\mathbf{A}_{12}$  is a  $(K-1)$ -dimensional vector, and  $a_{KK}$  is a scalar. To rewrite the second term, we note that

$$\mathbf{b}^T \boldsymbol{\theta} = \begin{pmatrix} \mathbf{b}^* \\ b_K \end{pmatrix}^T \begin{pmatrix} \boldsymbol{\theta}^* \\ -\frac{1}{f_K} \mathbf{f}^{*T} \boldsymbol{\theta}^* \end{pmatrix} = \mathbf{b}^{*T} \boldsymbol{\theta}^* - \frac{1}{f_K} b_K \mathbf{f}^{*T} \boldsymbol{\theta}^*$$

where  $\mathbf{b}^* = \{b_1, \dots, b_{K-1}\}$ . Therefore,

$$\begin{aligned} & \int_{\mathbf{f}^T \boldsymbol{\theta} = 0} \exp\left\{-\frac{1}{2\sigma^2}(\boldsymbol{\theta}^T \mathbf{A} \boldsymbol{\theta} - 2\mathbf{b}^T \boldsymbol{\theta})\right\} d\boldsymbol{\theta} \\ &= \int_{\boldsymbol{\theta}^*} \exp\left\{-\frac{1}{2\sigma^2}(\boldsymbol{\theta}^{*T} \mathbf{A}^* \boldsymbol{\theta}^* - 2\tilde{\mathbf{b}}^{*T} \boldsymbol{\theta}^*)\right\} d\boldsymbol{\theta}^* \\ &= \exp\left\{\frac{1}{2\sigma^2} \tilde{\mathbf{b}}^{*T} \mathbf{A}^{*-1} \tilde{\mathbf{b}}^*\right\} \int \exp\left\{-\frac{1}{2\sigma^2}(\boldsymbol{\theta}^* - \mathbf{A}^{*-1} \tilde{\mathbf{b}}^*)^T \mathbf{A}^* (\boldsymbol{\theta}^* - \mathbf{A}^{*-1} \tilde{\mathbf{b}}^*)\right\} d\boldsymbol{\theta}^* \\ &= \exp\left\{\frac{1}{2\sigma^2} \tilde{\mathbf{b}}^{*T} \mathbf{A}^{*-1} \tilde{\mathbf{b}}^*\right\} \times (2\pi\sigma^2)^{\frac{K-1}{2}} \{\det(\mathbf{A}^*)\}^{-\frac{1}{2}} \end{aligned} \quad (15)$$

where  $\mathbf{A}^* = \mathbf{A}_{11} - \frac{1}{f_K}(\mathbf{A}_{12} \mathbf{f}^{*T} + \mathbf{f}^* \mathbf{A}_{12}^T) + \frac{a_{KK}}{f_K^2} \mathbf{f}^* \mathbf{f}^{*T}$  and  $\tilde{\mathbf{b}} = \mathbf{b}^* - \frac{b_K}{f_K} \mathbf{f}$ . Combining equations (12)–(15), we obtain the marginal posterior distribution of  $\mathbf{y}$  as

$$\begin{aligned} f(\mathbf{y}|\sigma^2, \gamma^2, \mathbf{z}, \mathbf{X}) &= (2\pi\sigma^2)^{-n/2} \left(\frac{\sigma^2}{\gamma^2}\right)^{\frac{(K-1)}{2}} \{\det(\mathbf{A}^*)\}^{-\frac{1}{2}} \frac{\sqrt{\sum_{k=1}^K f_k^2}}{f_K} \\ &\quad \times \exp\left\{-\frac{1}{2\sigma^2}(\mathbf{y}^T \mathbf{y} - \tilde{\mathbf{b}}^{*T} (\mathbf{A}^*)^{-1} \tilde{\mathbf{b}}^*)\right\}. \end{aligned} \quad (16)$$

### 2.3.2 Sampling the cluster parameters $\boldsymbol{\theta}$

The  $K$ -vector of cluster parameters  $\boldsymbol{\theta}$  can be sampled from its posterior full conditional distribution, given  $\mathbf{z}$ ,  $\sigma^2$ ,  $\gamma^2$ , and  $\alpha$ :

$$\begin{aligned} f(\boldsymbol{\theta}|\mathbf{z}, \sigma^2, \gamma^2, \alpha) &\propto f(\boldsymbol{\theta}|\mathbf{z}, \gamma^2) f(\mathbf{y}|\boldsymbol{\theta}, \mathbf{z}, \sigma^2) \\ &\propto \exp\left(-\frac{1}{2\gamma^2} \boldsymbol{\theta}^T \boldsymbol{\theta}\right) I(\mathbf{f}^T \boldsymbol{\theta} = 0) \times \exp\left\{-\frac{1}{2\sigma^2}(\mathbf{y} - \mathbf{X}_z \boldsymbol{\theta})^T (\mathbf{y} - \mathbf{X}_z \boldsymbol{\theta})\right\} \\ &\propto \exp\left\{-\frac{1}{2}\left(\boldsymbol{\theta}^T \boldsymbol{\Sigma}_{\boldsymbol{\theta}}^{-1} \boldsymbol{\theta} - \frac{2}{\sigma^2} \mathbf{y}^T \mathbf{X}_z \boldsymbol{\theta}\right)\right\} I(\mathbf{f}^T \boldsymbol{\theta} = 0), \end{aligned} \quad (17)$$

which is a truncated normal density  $\mathcal{TN}(\boldsymbol{\mu}_\theta, \boldsymbol{\Sigma}_\theta, \mathbf{f}^T, 0)$  with  $\boldsymbol{\mu}_\theta = \boldsymbol{\Sigma}_\theta \frac{1}{\sigma^2} \mathbf{X}_z^T \mathbf{y}$  and  $\boldsymbol{\Sigma}_\theta = \left( \frac{1}{\gamma^2} \mathbf{I} + \frac{1}{\sigma^2} \mathbf{X}_z^T \mathbf{X}_z \right)^{-1}$ , as defined in equation (6). It is important to note that the posterior conditional of  $\boldsymbol{\theta}$  is constrained to the simplex  $\mathbf{f}^T \boldsymbol{\theta} = 0$ , implying that the posterior conditional of  $\boldsymbol{\beta}$  is compositionally constrained, i.e.,  $\mathbf{1}^T \boldsymbol{\beta} = 0$ . Next, we consider the challenging problem of simulating the hyperplane truncated random vector  $\boldsymbol{\theta}$  subject to the linear constraint  $\mathbf{f}^T \boldsymbol{\theta} = 0$ . In the following proposition, we present the well-known result that computes the posterior distribution of a conditional Gaussian vector with linear equality constraints.

**Proposition 1** *Let  $\tilde{\boldsymbol{\theta}}$  be a vector following a  $p$ -dimensional multivariate normal distribution with mean  $\boldsymbol{\mu}_{\tilde{\boldsymbol{\theta}}}$  and covariance matrix  $\boldsymbol{\Sigma}_{\tilde{\boldsymbol{\theta}}}$ . Then, the conditional distribution of  $\tilde{\boldsymbol{\theta}}$  given  $\mathbf{H}\tilde{\boldsymbol{\theta}} = \mathbf{q}$  is  $\mathcal{N}_p(\boldsymbol{\mu}_\mathcal{T}, \boldsymbol{\Sigma}_\mathcal{T})$ , where*

$$\begin{aligned} \boldsymbol{\mu}_\mathcal{T} &= \boldsymbol{\mu}_{\tilde{\boldsymbol{\theta}}} + \boldsymbol{\Sigma}_{\tilde{\boldsymbol{\theta}}} \mathbf{H}^T (\mathbf{H} \boldsymbol{\Sigma}_{\tilde{\boldsymbol{\theta}}} \mathbf{H}^T)^{-1} (\mathbf{q} - \mathbf{H} \boldsymbol{\mu}_{\tilde{\boldsymbol{\theta}}}) \\ \boldsymbol{\Sigma}_\mathcal{T} &= \boldsymbol{\Sigma}_{\tilde{\boldsymbol{\theta}}} - \boldsymbol{\Sigma}_{\tilde{\boldsymbol{\theta}}} \mathbf{H}^T (\mathbf{H} \boldsymbol{\Sigma}_{\tilde{\boldsymbol{\theta}}} \mathbf{H}^T)^{-1} \mathbf{H} \boldsymbol{\Sigma}_{\tilde{\boldsymbol{\theta}}}. \end{aligned}$$

The proof of the proposition follows classic derivations from multivariate statistics (Doucet 2010). The standard approach to simulate a truncated normal random vector  $\boldsymbol{\theta}$  from  $\mathcal{N}(\boldsymbol{\mu}_\mathcal{T}, \boldsymbol{\Sigma}_\mathcal{T})$  involves finding a Cholesky decomposition of  $\boldsymbol{\Sigma}_\mathcal{T}$  such that  $\boldsymbol{\Sigma}_\mathcal{T} = \mathbf{L}\mathbf{L}^T$ , where  $\mathbf{L}$  is a  $k \times k$  lower triangular matrix. However, this approach is computationally intensive. Therefore, we instead use the fast simulation approach detailed in Cong et al. (2017) to simulate from  $\mathcal{N}(\boldsymbol{\mu}_\mathcal{T}, \boldsymbol{\Sigma}_\mathcal{T})$ . This algorithm can be used to efficiently simulate a sum-constrained random vector  $\boldsymbol{\theta}$  from  $\tilde{\boldsymbol{\theta}}$ , where  $\boldsymbol{\theta} = \tilde{\boldsymbol{\theta}} + \boldsymbol{\Sigma}_{\tilde{\boldsymbol{\theta}}} \mathbf{H}^T (\mathbf{H} \boldsymbol{\Sigma}_{\tilde{\boldsymbol{\theta}}} \mathbf{H}^T)^{-1} (\mathbf{q} - \mathbf{H}\tilde{\boldsymbol{\theta}})$ , using  $\tilde{\boldsymbol{\theta}} \sim \mathcal{N}(\boldsymbol{\mu}_{\tilde{\boldsymbol{\theta}}}, \boldsymbol{\Sigma}_{\tilde{\boldsymbol{\theta}}})$ . For complete details and technical proofs of the algorithm refer to Cong et al. (2017).

### 2.3.3 Sample the variance parameter $\gamma^2$

To sample the variance parameter  $\gamma^2$ , we compute its posterior full conditional as

$$\begin{aligned} p(\gamma^2 \mid \boldsymbol{\theta}, \mathbf{z}, \alpha, \sigma^2) &\propto p(\boldsymbol{\theta}, \mathbf{z} \mid \gamma^2) \cdot p(\gamma^2) \\ &= \left\{ \frac{\exp\left(-\frac{1}{2\gamma^2} \boldsymbol{\theta}^T \boldsymbol{\theta}\right)}{\int_{\mathbf{H}\boldsymbol{\theta}=\mathbf{q}} \exp\left(-\frac{1}{2\gamma^2} \boldsymbol{\theta}^T \boldsymbol{\theta}\right) d\boldsymbol{\theta}} \right\} \times \left\{ \frac{b_\gamma^{a_\gamma}}{\Gamma(a_\gamma)} (\gamma^2)^{-a_\gamma-1} \exp\left(-\frac{b_\gamma}{\gamma^2}\right) \right\} \\ &\propto (\gamma^2)^{-a_\gamma-(K-1)/2-1} \exp\left(-\frac{1}{2\gamma^2} \boldsymbol{\theta}^T \boldsymbol{\theta} - \frac{b_\gamma}{\gamma^2}\right), \end{aligned} \quad (18)$$

Therefore, equation (18) is an unnormalized inverse gamma density  $\mathcal{IG}(a_\gamma + (K-1)/2, b_\gamma + 0.5\boldsymbol{\theta}^T \boldsymbol{\theta})$ .

### 2.3.4 Sampling the variance $\sigma^2$ and concentration $\alpha$

The inverse gamma prior on  $\sigma^2$  allows for Gibbs updates of  $\sigma^2$ . Its posterior conditional is an inverse gamma density  $\mathcal{IG}(a_\sigma + n/2, b_\sigma + 0.5(\mathbf{y} - \mathbf{X}_z \boldsymbol{\theta})^T (\mathbf{y} - \mathbf{X}_z \boldsymbol{\theta}))$ . We have a non-informative Gamma prior on the concentration parameter,  $\alpha \sim \text{Gamma}(a_\alpha, b_\alpha)$ , and update it using the method outlined in Escobar & West (1995). Finally, we set  $\alpha_0 = 2$  which is equivalent to  $\psi_0 \sim \text{Uniform}(0, 1)$ . Having a uniform non-informative prior on  $\psi_0$  allows flexibility in our belief about the number of non-zero coefficients in the model.

## 3 Simulation studies

In this section, we benchmark the performance of BRACE against alternative compositional regression methods. We also assess the performance of BRACE in recovering the ground truth clusters.

### 3.1 General setup

We start by sampling an  $n \times p$  data matrix  $\mathbf{U}$  from a multivariate normal distribution  $N_p(\boldsymbol{\theta}, \boldsymbol{\Sigma})$ , and obtain the relative abundance matrix as  $\mathbf{O} = \exp(\mathbf{U}) / \mathbf{1}^T \exp(\mathbf{U})$ . Using this transformation, the variables follow a logistic normal distribution (?), a commonly used distribution for modeling microbial abundances. In order to create microbiome features with varying abundance, we set  $\theta_j = \log(0.5p)$  for  $j = 1, \dots, 10$ , and 0 otherwise, and we assume a covariance structure given by  $\boldsymbol{\Sigma}$ . Finally, we generate the responses as  $\mathbf{y} = \mathbf{X}\boldsymbol{\beta} + \boldsymbol{\varepsilon}$ , where  $\boldsymbol{\beta}$  is the vector of regression coefficients and  $\mathbf{X} = \log(\mathbf{O})$ . We consider settings with  $n = 300$  and  $p = 100, 300$ , and 1000. We generate  $\sigma$  so that the signal-to-noise ratio (SNR) is 5, where  $\text{SNR} = \text{mean}(|\beta_{\beta_j \neq 0}| / \sigma, j = 1, \dots, p)$ . For each setting, we generate 30 simulated datasets, and randomly partition the data into training and test samples with a ratio of 80 : 20. The model



is fitted on the training set, and the prediction error (PE) =  $\frac{1}{m_{\text{test}}}(\mathbf{y}_{\text{test}} - \mathbf{X}_{\text{test}}\hat{\beta}_{\text{train}})^T(\mathbf{y}_{\text{test}} - \mathbf{X}_{\text{test}}\hat{\beta}_{\text{train}})$  and  $l_2$  loss  $\|\beta_{\text{true}} - \hat{\beta}_{\text{train}}\|_2$  are calculated on the test set. This process is repeated for 30 simulated datasets, and the mean and standard deviations of the results are reported.

We fit BRACE to each simulated training data set using the Gibbs sampler described in Section 2.3, run for 5000 iterations, with the first 3000 iterations used as burn-in. For all simulation settings, we use the non-informative prior specifications:  $\gamma^2 \sim IG(0.001, 0.001)$ ,  $\sigma^2 \sim IG(0.001, 0.001)$ ,  $a_\alpha = 1/(0.75 \log p)^2$ , and  $b_\alpha = a_\alpha/\sqrt{p}$ . This prior specification for  $\alpha$  allows flexibility in the number of clusters. A detailed discussion on the choice of priors for  $\alpha$  can be found in Escobar & West (1995) and Nott (2008).

### 3.2 Benchmarking methods

We compare the performance of BRACE with that of the following existing approaches: **lasso CLR**, which performs lasso regression (Tibshirani 1996) on predictors transformed using the centered log ratio (CLR) transformation (Aitchison & Bacon-Shone 1984), **lasso comp**, which is a penalized compositional regression approach proposed by Lin et al. (2014), **BAZE**, a Bayesian variable selection for compositional data (Zhang et al. 2021) and **BCGLM**, a Bayesian variable selection for generalized regression model with compositional predictors (Zhang et al. 2024). We now describe the parameter settings we used for the benchmarking models. For the Bayesian models, we adopted standard hyperpriors as recommended by the authors. In the case of BCGLM, results remained consistent when varying  $m_0$ , the prior guess of the number of relevant predictors. Therefore, we set  $m_0 = 10$ . For BAZE, which relies on a phylogenetic tree-based similarity matrix  $\mathbf{Q}$  to capture the similarity between taxa,  $\mathbf{Q}$  was defined as a diagonal matrix to reflect a lack of prior information. For the frequentist approaches, lasso comp and lasso CLR, cross-validation was used to select the hyperparameters.

To evaluate the variable selection and coefficient clustering performance of our proposed approach we designed two simulation scenarios having different covariance structures between the compositional predictors.

### 3.3 Structure of $\beta$ and $\Sigma$

We construct  $\beta$  with 35 nonzero elements across 9 clusters, with two clusters having only one element. The true parameter vector is given as  $\beta = \{-0.8_4, -1.41_6, -1.95_4, -1.16, 0.96, 0_3, 1.04_6, 0.51_4, 1.95_7, 0_{(p-37)}\}$ . It is to be noted that  $\beta$  sums to 1 and its components have varying degrees of magnitude, implying varying strengths of association between the predictors and the response. Given that correlations among microbiome features frequently occur in practice, we examine two settings involving dependent predictors to better replicate real-world scenarios.

- Case Dep1: We introduce uniform correlation in the data generation procedure by setting  $\Sigma_{i,j} = \rho^{|i-j|}$  with  $\rho = 0.5$ . This setting ensures that the correlation between predictors decreases as the distance between them increases.
- Case Dep2: To capture varying levels of correlation among predictors within and between clusters, we set the within-cluster correlations to  $\Sigma_{i,j_{wc}} = 0.75 - 0.015 \times |i - j|$ , making the correlation between two covariates within the same cluster inversely proportional to their distance (with a maximum of 0.75). Additionally, we define the between-cluster correlations among the predictors as  $\Sigma_{i,j_{bc}} = 0.4 - 0.02 \times |i - j|$ . The coefficients for the other non-diagonal elements are set to 0 and the diagonal elements of  $\Sigma$  are set to 1.

Table 1 displays the performance metrics, including prediction error, coefficient estimation accuracy, and number of false positives and false negatives, for the setting with  $\rho = 0.5$ . BRACE outperforms the competing Bayesian models BAZE and BCGLM in terms of test set prediction error and L2 loss. BAZE closely follows BRACE in these two metrics but exhibits a slightly high average false negative in the case  $p = 300$ . It is worth noting that BCGLM, implemented in STAN, is computationally intensive, requiring 10 hours to run a single replicate for  $p = 1000$ . Therefore, the average results for BCGLM in these cases are based on only 10 random replicates instead of 30, and it has the worst performance among all Bayesian approaches. All the frequentist methods perform badly for all the metrics with compositional lasso exhibiting a competitive performance in the  $p = 100$  case. BRACE performs well in both the low and high-dimensional setups.

Table 2 presents the performance metrics for the case Dep2, where different covariance structures are used for within and between cluster covariances. Similar to Dep1, BRACE exhibits strong performance in terms of prediction error in this setup. Notably, BCGLM shows an exceptionally high computation time for  $p = 1000$  which limits the results to 10 replicates. As expected, based on the results from the previous dependent setup, the frequentist methods generally do not perform competitively, with the sole exception of lasso comp in the  $p = 100$  case. The robust performance of BRACE in this complex, real-world-like setting highlights its applicability to microbiome studies, where clustering many rare features could lead to improved prediction outcomes. Overall, BRACE demonstrates strong performance in

terms of out-of-sample prediction error and false positive error control, outperforming the alternative methods in the majority of the simulation settings.

Since this simulation setting was the most challenging computationally, we considered it as a benchmark study for comparing the computational cost of the methods considered. We found that for the setting with  $p = 100$ , BCGLM required the longest run times (95 seconds for 1000 MCMC iterations), followed by BRACE (75 seconds for 1000 MCMC iterations). The penalized methods and BAZE were more computationally efficient.

**Table 1:** Performance comparison for simulated data with dependent covariates using  $\rho = 0.5$ , sample size  $n = 300$ , and  $\text{SNR} = 1$ . Performance is summarized in terms of prediction error (PE), L2 loss in estimation of the coefficient vector, and number of false positives (FP) and false negatives (FN). Entries that reflect the smallest PE and L2 loss are marked in bold.

	Method	PE	L2 Loss	FP	FN
p = 100	lasso CLR	706.1 (129.5)	8.59 (0.28)	0.00 (0.00)	32.48 (1.13)
	lasso constrained	9162.6 (614.6)	0.43 (0.05)	29.4 (6.56)	0.00 (0.00)
	lasso comp	6.82 (1.62)	1.22 (0.16)	1.72 (1.68)	0.01 (0.1)
	BAZE	1.87 (0.16)	0.45 (0.06)	0.00 (0.00)	0.00 (0.00)
	BCGLM	2.23 (0.33)	0.27 (0.02)	1.92 (1.86)	0.00 (0.00)
	<b>BRACE</b>	<b>1.58</b> (0.15)	<b>0.25</b> (0.05)	0.00 (0.00)	0.00 (0.00)
p = 300	lasso CLR	14044 (860.6)	0.54 (0.08)	16.74 (5.28)	0.00 (0.00)
	lasso constrained	717.4 (129.9)	8.59 (0.31)	0.00 (0.00)	32.31 (1.13)
	lasso comp	588.4 (113.0)	6.71(0.31)	1.27 (1.40)	16.52 (1.96)
	BAZE	1.84 (0.21)	0.36 (0.04)	0.00 (0.00)	0.05 (0.21)
	BCGLM	4.07 (0.81)	0.37 (0.01)	1.55 (1.56)	0.01 (0.10)
	<b>BRACE</b>	<b>1.79</b> (0.20)	<b>0.30</b> (0.04)	0.00 (0.00)	0.00 (0.00)
p = 1000	lasso CLR	20923 (1035.8)	0.60 (0.07)	40.04 (8.72)	0.00 (0.00)
	lasso constrained	718.7 (133.7)	8.63 (0.40)	0.00 (0.00)	32.25 (1.16)
	lasso comp	737.5 (117.3)	6.95 (0.35)	4.39 (3.12)	17.67 (1.84)
	BAZE	1.93 (0.21)	0.35 (0.03)	0.00 (0.00)	0.00 (0.00)
	BCGLM	29.77 (12.65)	0.36 (0.06)	0.00 (0.00)	9.67 (2.08)
	<b>BRACE</b>	<b>1.86</b> (0.17)	<b>0.29</b> (0.03)	0.00 (0.00)	0.00 (0.00)

**Table 2:** Performance comparison for simulated data with dependent covariates with different between and within cluster covariance setup, **sample size**  $n = 300$ , and  $\text{SNR} = 1$ . Performance is summarized in terms of prediction error (PE), L2 loss in estimation of the coefficient vector, and number of false positives (FP) and false negatives (FN). Entries that reflect the smallest PE and L2 loss are marked in bold.

	Method	PE	L2 Loss	FP	FN
p = 100	lasso CLR	12472 (1804.1)	0.39 (0.05)	0.04 (0.02)	0.00 (0.00)
	lasso constrained	3918.1 (908.0)	8.43 (0.29)	0.04 (0.2)	32.64 (1.12)
	lasso comp	4.02 (1.04)	0.43 (0.07)	0.80 (0.95)	0.00 (0.00)
	BAZE	2.16 (0.19)	0.24 (0.03)	0.00 (0.00)	0.00 (0.00)
	BCGLM	2.47 (0.34)	0.20 (0.01)	1.64 (1.52)	0.00 (0.00)
	<b>BRACE</b>	<b>2.04</b> (0.19)	<b>0.18</b> (0.04)	0.00 (0.00)	0.00 (0.00)
p = 300	lasso CLR	17715 (2110.5)	0.48 (0.06)	0.05 (0.22)	0.00 (0.00)
	lasso constrained	3989.8 (754.0)	8.62(0.56)	0.15 (0.36)	32.64(1.15)
	lasso comp	1360.3 (283.8)	6.40 (0.25)	0.00 (0.00)	16.88 (1.46)
	BAZE	2.59 (0.19)	0.42 (0.05)	0.00 (0.00)	0.00 (0.00)
	BCGLM	2.47 (0.34)	0.21 (0.01)	2.40 (2.56)	0.00 (0.00)
	<b>BRACE</b>	<b>2.07</b> (0.19)	<b>0.19</b> (0.04)	0.00 (0.00)	0.00 (0.00)
p = 1000	lasso CLR	25016.4 (2782.8)	0.49 (0.05)	0.2 (0.53)	0.00 (0.00)
	lasso constrained	4216.4 (612.7)	8.81 (0.86)	0.05 (0.23)	32.89 (1.08)
	lasso comp	1491.1 (334.6)	6.52 (0.31)	0.00 (0.00)	17.35 (1.66)
	BAZE	2.23 (0.19)	0.17 (0.03)	0.00 (0.00)	0.00 (0.00)
	BCGLM	21.756 (17.0)	0.11 (0.03)	0.00 (0.00)	12.5 (3.53)
	<b>BRACE</b>	<b>2.12</b> (0.24)	0.17 (0.04)	0.00 (0.00)	0.00 (0.00)

### 3.4 Clustering accuracy

In addition to variable selection and prediction, our proposed model facilitates the grouping of similar features through clustering of regression coefficients. In this subsection, we evaluate the clustering concordance between the true and predicted cluster labels. We obtain a single set of predicted labels from our MCMC samples using the SALSO algorithm, which identifies the clustering that minimizes the posterior expected loss given a sequence of sampled labels (Dahl et al. 2022). As recommended by the authors of SALSO, we use the generalized variation of information (VI) loss for the optimization function. We compare the predicted cluster labels to the true cluster labels in the simulation setup using the adjusted Rand index (ARI), which has an expected value of 0 under a random assignment of labels and a value of 1 under perfect agreement. Given a set  $\mathbf{S}$  of  $n$  elements, and two clusterings of these elements, namely the true cluster labels  $\mathbf{c} = \{c_1, \dots, c_{K_1}\}$  and predicted cluster labels  $\mathbf{z} = \{z_1, \dots, z_{K_2}\}$ , the overlap between  $\mathbf{c}$  and  $\mathbf{z}$  can be summarized in a contingency table  $[n_{k_1 k_2}]$ , where each entry  $n_{k_1 k_2}$  denotes the number of objects in common between  $c_{k_1}$  and  $z_{k_2}$ :  $n_{k_1 k_2} = |c_{k_1} \cap z_{k_2}|$ . The adjusted Rand index is given as

$$ARI = \frac{\sum_{k_1 k_2} \binom{n_{k_1 k_2}}{2} - \left[ \sum_{k_1} \binom{a_{k_1}}{2} \sum_{k_2} \binom{b_{k_2}}{2} \right] / \binom{n}{2}}{\frac{1}{2} \left[ \sum_{k_1} \binom{a_{k_1}}{2} + \sum_{k_2} \binom{b_{k_2}}{2} \right] - \left[ \sum_{k_1} \binom{a_{k_1}}{2} \sum_{k_2} \binom{b_{k_2}}{2} \right] / \binom{n}{2}}, \quad (19)$$

where  $n$  is the total number of objects being clustered,  $n_{ij}$  is the number of pairs of objects that belong to the same cluster in both the true and predicted clustering,  $a_{k_1}$  is the number of objects in the true cluster  $k_1$ , and  $b_{k_2}$  is the number of objects in the predicted cluster  $k_2$ . Figure 2 shows the clustering performance of our proposed method for the two simulation scenarios with dependent predictors and the number of predictors set to  $p = 100, 300$ , and  $1000$ . The mean clustering accuracy decreases with an increase in the number of predictors as the size of the true null cluster increases and it becomes increasingly difficult for the model to correctly predict the clustering labels of the elements belonging to the non-null clusters. The ARI for the dependent case Dep2 is lower than for the Dep1 case, highlighting the complexity of case Dep2 over Dep1. Overall, BRACE achieves high values of the ARI for all cases, indicating its ability to recover the true cluster labels with high accuracy.

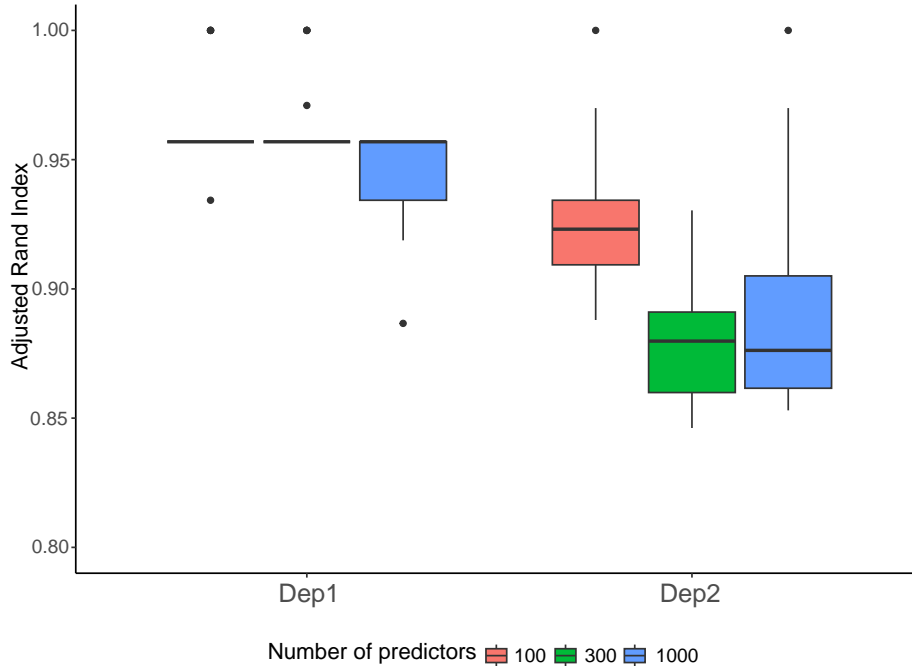


**Figure 2:** Boxplots showing the adjusted Rand indices calculated by comparing the true and predicted cluster labels in the two dependent setup with the number of predictors set to  $p = 100, 300$ , and  $1000$ .

## 4 Application to oral microbiome data

To illustrate the utility of our proposed method, we applied it to data from the Oral Infections, Glucose Intolerance, and Insulin Resistance Study (ORIGINS), which investigated the correlation between periodontal microbiota and insulin resistance (Demmer et al. 2017). Previous studies have established a significant association between periodontitis,

a chronic inflammatory disease affecting the tissues supporting the teeth, and the risk of type 2 diabetes. Type 2 diabetes, constituting 90% of diabetes cases, arises from disruptions in glucose regulation and insulin resistance. The cross-sectional ORIGINS study included 152 adults without diabetes (77% female), aged 20–55 years. The Human Oral Microbe Identification Microarray (Colombo et al. 2009) was used to quantify the abundance of 379 taxa in subgingival plaque samples. For this case study, we obtained the microbiome profiling data from Demmer et al. (2017). We utilized the observed insulin levels as our response variable, employing our proposed method to elucidate the relationship between the periodontal microbiome and insulin levels. We filtered the dataset to exclude samples lacking insulin level information and taxa with a total abundance lower than 30, resulting in 130 taxa and 111 samples. After filtering, there were no repeated measures (i.e., each sample corresponds to a unique subject). We replaced exact zeros in the count data with a small pseudocount of 0.5. We then transformed the counts into relative abundances and applied a log transformation to form the predictor matrix.

#### 4.1 Prediction, selection and clustering results

We randomly divided the 111 samples into a training set of 83 samples and a test set of 28 samples, and fit the proposed and benchmarking models on the training data. The process was repeated for 10 independent replicates, and we utilized these fitted models to calculate the prediction error on the test sets. The mean and standard deviation (in parentheses) of the prediction errors for the 10 replicates were 27.34 (9.63) for lasso CLR, 27.52 (9.67) for lasso comp, 25.38 (10.19) for BCGLM, 25.76 (10.84) for BAZE and 24.70 (10.71) for BRACE. This sample-splitting approach supports the utility of our proposed method in accurately identifying true patterns of microbiome association, and is consistent with our simulation results in that the proposed method achieves the lowest prediction error across the methods considered.

To gain further insights into the role of oral microbiome composition in regulating insulin levels, we fit the proposed model on the full data. We obtained a final clustering from the sampled cluster labels for our model using SALSO as described in Section 4.1. To facilitate variable selection, we filtered out features that contained zero within their 95% posterior credible intervals, and finally identified 25 features grouped into seven nonzero clusters, as illustrated in Figure 3. Species belonging to phyla Firmicutes and Bacteroidota to found to be associated with insulin levels. At the genus level, BRACE identified species belonging to *Porphyromonas*, *Tannerella*, and *Treponema*. We now discuss the findings in more detail, focusing on the bacterial species that confer increased risk. A cluster of four species was identified as having the strongest positive association with increased insulin levels. Within this cluster, *Tannerella forsythia* has long been recognized as one of the bacteria that contribute to periodontitis (Socransky et al. 1998); more recently, increased abundance of *T. forsythia* in the oral microbiome has been associated with higher fasting blood glucose levels (Chang et al. 2023). This cluster also included a species belonging to the genus *Prevotella*, which supports the general understanding that *Prevotella* species contribute to increased inflammation (Könönen et al. 2022). Traditionally *Tannerella forsythia* along with *Treponema denticola* and *Porphyromonas gingivalis* species are believed to play a pathogenic role in periodontitis. However in a similar finding from the ORIGINS study we observed no association with *P. gingivalis* and an inverse association between *T. denticola* and insulin resistance. These findings could be data specific or suggest that the abundance of these species may rise as a response to host changes, such as overt hyperglycemia or periodontal disease, becoming relevant to systemic inflammation and insulin resistance only at more advanced stages of periodontal disease and dysglycemia (Demmer et al. 2017).

Finally, to assess whether BRACE estimated clusters represented functionally distinct characteristics, we conducted further analysis on the functional abundances of the taxa, obtained using PICRUSt (Douglas et al. 2020), within each cluster. UMAP analysis of the functional feature distributions across the six clusters identified by BRACE revealed notable differences in functional abundances. This observation was further supported by MANOVA performed on the UMAP coordinates, which yielded a significant p-value ( $p$  value  $< 0.01$ ), as illustrated in Figure 4. These results suggest that BRACE effectively identifies clusters with distinct functional roles associated with the outcome, and strengthens confidence in BRACE’s ability to reveal biologically meaningful patterns within the data.

#### 4.2 Concordance of cluster labels to phylogeny

Our next goal was to investigate whether the taxa clusters identified by BRACE demonstrated phylogenetic similarity. To achieve that goal, we first constructed a phylogenetic tree based on the representative sequences for the observed taxa. Next, we calculated the phylogenetic correlation matrix  $\mathbf{R}$  using the formula  $r_{ij} = \frac{l_{ij}}{\sqrt{l_{ii}}\sqrt{l_{jj}}}$ , where  $l_{aa}$  is defined as the branch length from the leaf node  $a$  to the root node, for  $a = 1, \dots, p$ , and  $l_{ij}$  is the shared branch length between leaf nodes  $i$  and  $j$ . This matrix was calculated using the R package ape (Paradis & Schliep 2019). Next, given the estimated cluster labels, we calculated the within and between-cluster mean phylogenetic correlations given in Figure 5, the hypothesis being that the within-cluster phylogenetic correlations will be higher than the between-cluster ones in most cases. The proportion of times the within-cluster correlations was greater than the between-cluster correlations, for all features, is 0.67, 1.00, 0.83, 1.00, 1.00, 1.00, 1.00. This result demonstrates that our model’s clustering scheme successfully captures some phylogenetic similarity between the taxa, without the need to prespecify this information

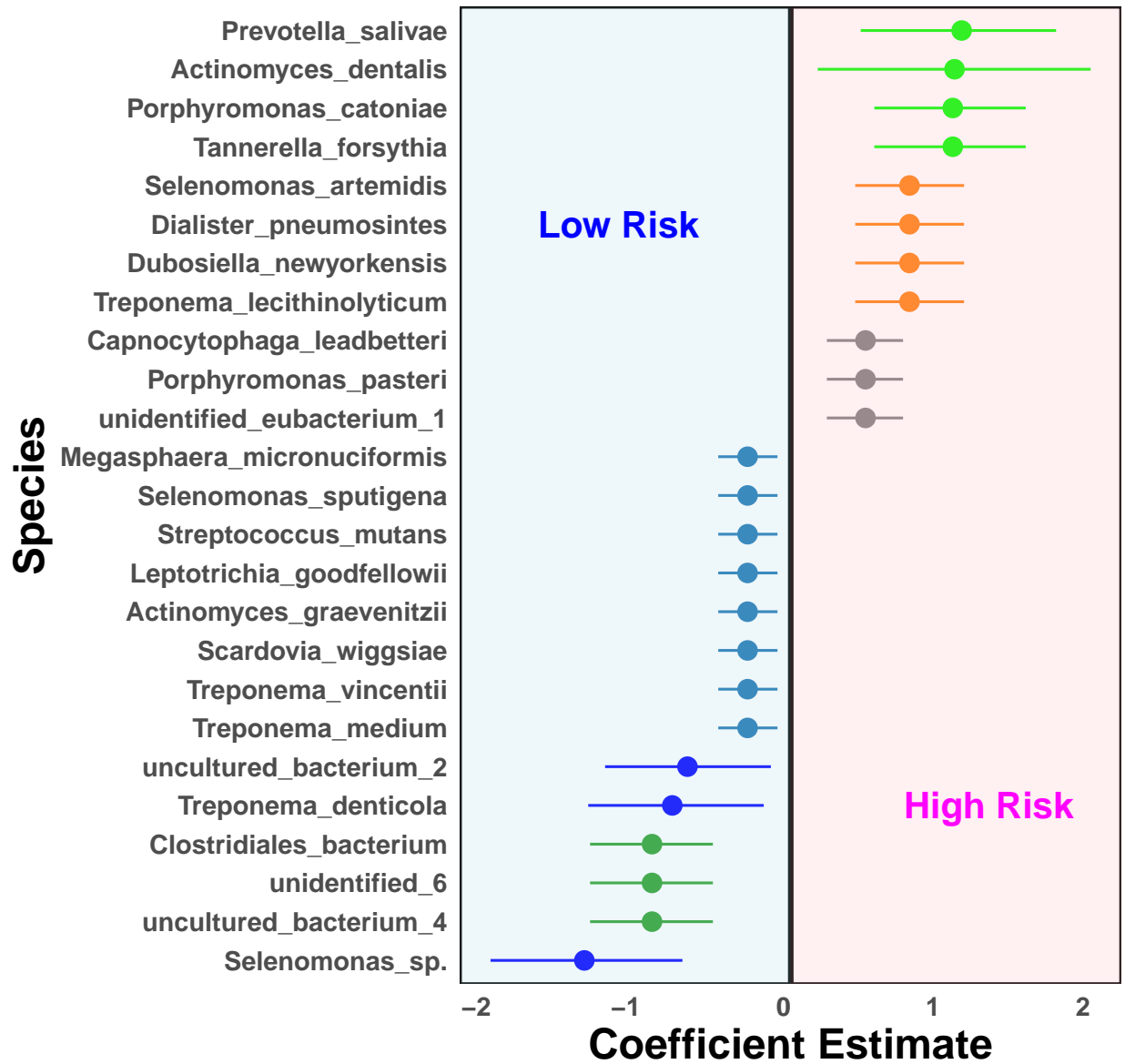


**Figure 3:** Parameter estimates and credible intervals for all features selected by BRACE. The color of the dots determines the cluster labels of the estimates.

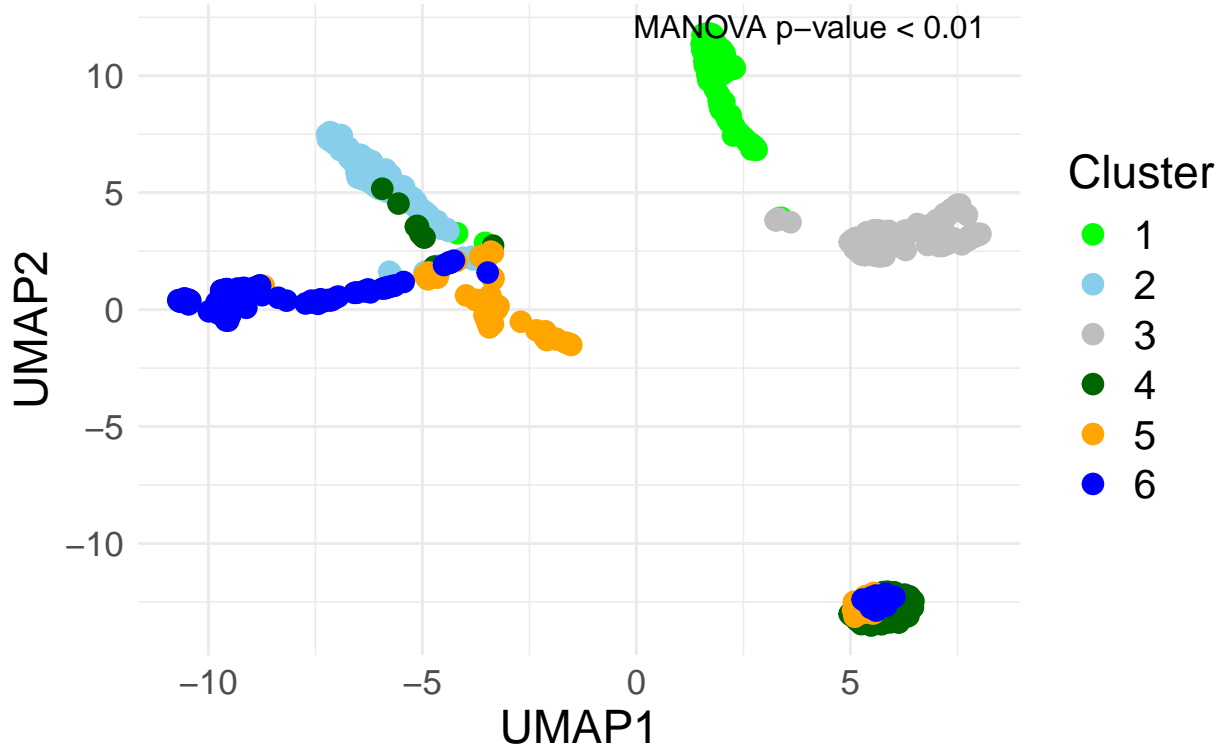


**Figure 4:** UMAP visualization of functional feature distributions across six clusters identified by BRACE and refined with SALSO partitioning. A MANOVA analysis on the UMAP coordinates yielded a significant p-value ( $p < 0.01$ ), indicating significant differences in functional abundances across clusters.

as a model input. In combination with the functional similarity results, we conclude that the clusters identified by BRACE exhibit greater phylogenetic similarity within clusters than between clusters, while also capturing functional information on shared effects.

## 5 Discussion

In this article, we present a novel statistical approach for microbiome compositional regression utilizing a nonparametric Bayesian approach for dimension reduction. Our proposed methodology represents a significant advancement in regression modeling of microbiome data for two key reasons. First, it introduces the inaugural application of Dirichlet process models for high-dimensional compositional regression with flexible microbiome feature aggregation and selection. Second, we develop a novel approach to address the compositional constraint in estimation of the regression coefficients. Through a combination of simulations and real data analysis, we illustrate the superior estimation and prediction performance of our proposed model compared to existing methods.

Our proposed method can be extended to incorporate additional covariates, which could be relevant for many health-related studies. To accommodate additional clinical or demographic variables we can write  $\mathbf{y} = \mathbf{X}\boldsymbol{\beta} + \mathbf{C}\boldsymbol{\zeta} + \boldsymbol{\varepsilon}$ , where  $\mathbf{C}$  is the matrix of additional covariates and  $\boldsymbol{\zeta} \sim N(\mathbf{0}, \sigma_{\boldsymbol{\zeta}}^2 \mathbf{I})$ . In addition, our formulation can be extended to model binary or count responses by changing the linear link function to probit/logit or log, but these extensions are non-trivial and will be explored in future work.

Finally, one of the main limitations of our work is the computational burden of inverting high-dimensional matrices while updating the cluster labels. The collapsed Gibbs sampler used in this paper is not scalable for high-dimensional cases if there is a large number of clusters in the data. Computational scalability can only be achieved when the number of clusters  $k \ll p$ , the number of predictors; therefore, we recommend that the Gibbs sampler be initialized with a small number of clusters. Faster methods that utilize approximation algorithms for DP priors, like variational Bayes approaches, have the potential to make our methodology more scalable for larger data sets with many clusters.

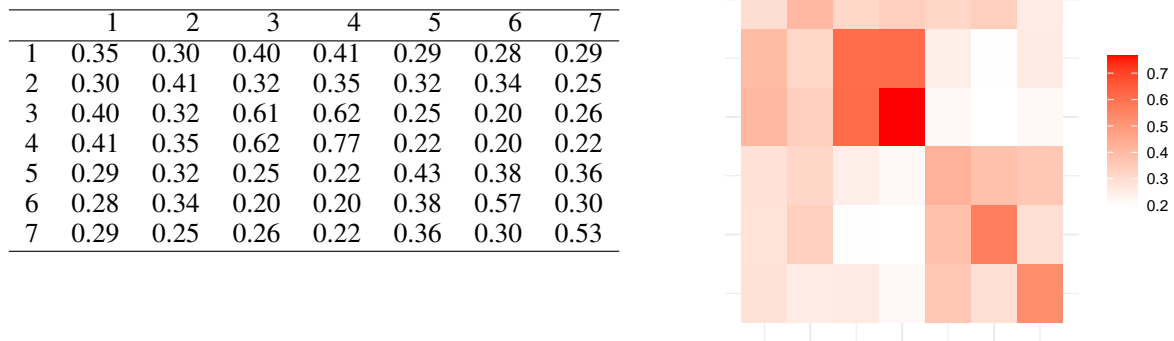


**Figure 5:** Table and heatmap showing the average phylogenetic correlations within and between the clusters for selected features.

## References

- Aitchison, J. & Bacon-Shone, J. (1984), ‘Log contrast models for experiments with mixtures’, *Biometrika* **71**(2), 323–330.
- Bien, J., Yan, X., Simpson, L. & Müller, C. L. (2021), ‘Tree-aggregated predictive modeling of microbiome data’, *Scientific Reports* **11**(1), 14505.
- Blackwell, D. & MacQueen, J. B. (1973), ‘Ferguson distributions via Pólya urn schemes’, *The Annals of Statistics* **1**(2), 353–355.
- Callahan, B. J., Sankaran, K., Fukuyama, J. A., McMurdie, P. J. & Holmes, S. P. (2016), ‘Bioconductor workflow for microbiome data analysis: from raw reads to community analyses’, *F1000Research* **5**.
- Chang, Y.-R., Cheng, W.-C., Hsiao, Y.-C., Su, G.-W., Lin, S.-J. et al. (2023), ‘Links between oral microbiome and insulin resistance: Involvement of MAP kinase signaling pathway’, *Biochimie* **214**, 134–144.
- Colombo, A., Boches, S., Cotton, S., Goodson, J., Kent, R. et al. (2009), ‘Comparisons of subgingival microbial profiles of refractory periodontitis, severe periodontitis, and periodontal health using the human oral microbe identification microarray’, *Journal of Periodontology* **80**, 1421–32.
- Cong, Y., Chen, B. & Zhou, M. (2017), ‘Fast simulation of hyperplane-truncated multivariate normal distributions’, *Bayesian Analysis* **12**(4), 1017–1037.
- Dahl, D. B., Johnson, D. J. & Müller, P. (2022), ‘Search algorithms and loss functions for Bayesian clustering’, *Journal of Computational and Graphical Statistics* **31**(4), 1189–1201.
- Demmer, R., Jacobs, D., Singh, R., Zuk, A., Rosenbaum, M. et al. (2015), ‘Periodontal bacteria and prediabetes prevalence in ORIGINS: the oral infections, glucose intolerance, and insulin resistance study’, *Journal of Dental Research* **94**(9\_suppl), 211S–211S.
- Demmer, R. T., Breskin, A., Rosenbaum, M., Zuk, A., LeDuc, C. et al. (2017), ‘The subgingival microbiome, systemic inflammation and insulin resistance: The Oral Infections, Glucose Intolerance and Insulin Resistance Study’, *Journal of Clinical Periodontology* **44**(3), 255–265.
- Doucet, A. (2010), ‘A note on efficient conditional simulation of Gaussian distributions’, *Departments of Computer Science and Statistics, University of British Columbia* **1020**.
- Douglas, G. M., Maffei, V. J., Zaneveld, J. R., Yurgel, S. N., Brown, J. R., Taylor, C. M., Huttenhower, C. & Langille, M. G. (2020), ‘Picrust2 for prediction of metagenome functions’, *Nature biotechnology* **38**(6), 685–688.
- Dunson, D. B., Herring, A. H. & Engel, S. M. (2008), ‘Bayesian selection and clustering of polymorphisms in functionally related genes’, *Journal of the American Statistical Association* **103**(482), 534–546.
- Escobar, M. D. & West, M. (1995), ‘Bayesian density estimation and inference using mixtures’, *Journal of the American Statistical Association* **90**(430), 577–588.
- Gloor, G. B., Macklaim, J. M., Pawlowsky-Glahn, V. & Egozcue, J. J. (2017), ‘Microbiome datasets are compositional: and this is not optional’, *Frontiers in Microbiology* **8**, 2224.

- Gurav, A. N. (2012), ‘Periodontitis and insulin resistance: casual or causal relationship?’, *Diabetes & Metabolism Journal* **36**(6), 404.
- Könönen, E., Fteita, D., Gursoy, U. K. & Gursoy, M. (2022), ‘*Prevotella* species as oral residents and infectious agents with potential impact on systemic conditions’, *Journal of Oral Microbiology* **14**(1), 2079814.
- Lin, W., Shi, P., Feng, R. & Li, H. (2014), ‘Variable selection in regression with compositional covariates’, *Biometrika* **101**(4), 785–797.
- Mehrotra, S. & Maity, A. (2022), ‘Simultaneous variable selection, clustering, and smoothing in function-on-scalar regression’, *Canadian Journal of Statistics* **50**(1), 180–199.
- Neal, R. M. (2000), ‘Markov chain sampling methods for Dirichlet process mixture models’, *Journal of Computational and Graphical Statistics* **9**(2), 249–265.
- Nott, D. J. (2008), ‘Predictive performance of Dirichlet process shrinkage methods in linear regression’, *Computational Statistics & Data Analysis* **52**(7), 3658–3669.
- Paradis, E. & Schliep, K. (2019), ‘ape 5.0: an environment for modern phylogenetics and evolutionary analyses in R’, *Bioinformatics* **35**, 526–528.
- Peterson, C. B., Saha, S. & Do, K.-A. (2024), ‘Analysis of microbiome data’, *Annual Review of Statistics and Its Application* **11**, 483–504.
- Pflughoeft, K. J. & Versalovic, J. (2012), ‘Human microbiome in health and disease’, *Annual Review of Pathology: Mechanisms of Disease* **7**, 99–122.
- Pihlstrom, B. L., Michalowicz, B. S. & Johnson, N. W. (2005), ‘Periodontal diseases’, *The Lancet* **366**(9499), 1809–1820.
- Shi, P., Zhang, A. & Li, H. (2016), ‘Regression analysis for microbiome compositional data’, *Annals of Applied Statistics* **10**(2), 1019–1040.
- Socransky, S., Haffajee, A., Cugini, M., Smith, C. & Kent Jr, R. (1998), ‘Microbial complexes in subgingival plaque’, *Journal of Clinical Periodontology* **25**(2), 134–144.
- Tibshirani, R. (1996), ‘Regression shrinkage and selection via the lasso’, *Journal of the Royal Statistical Society Series B: Statistical Methodology* **58**(1), 267–288.
- Yan, X. & Bien, J. (2021), ‘Rare feature selection in high dimensions’, *Journal of the American Statistical Association* **116**(534), 887–900.
- Zhang, L., Shi, Y., Jenq, R. R., Do, K.-A. & Peterson, C. B. (2021), ‘Bayesian compositional regression with structured priors for microbiome feature selection’, *Biometrics* **77**(3), 824–838.
- Zhang, L., Zhang, X. & Yi, N. (2024), ‘Bayesian compositional generalized linear models for analyzing microbiome data’, *Statistics in Medicine* **43**, 141–155.